

Influence of Atmospheric Rivers on Alaskan River Ice

Russ Limber^{1,2}, Elias C. Massoud², Bin Guan^{3,4}, Forrest M. Hoffman²,
Jitendra Kumar²

¹The University of Tennessee, Knoxville, Knoxville, TN, USA

²Oak Ridge National Laboratory, Oak Ridge, TN, USA

³Joint Institute for Regional Earth System Science and Engineering, University of California, Los Angeles,

Los Angeles, CA, USA

⁴Jet Propulsion Laboratory, California Institute of Technology, Pasadena, CA, USA

Key Points:

- Interannually, atmospheric rivers (ARs) can lead to a week-long persistent increase in daily air temperatures over Interior Alaska (AK)
- In AK, ARs account for 36% of annual precipitation, 57% of extreme precipitation and explain 48% of interannual variability of precipitation
- AR events during the coldest months delay the annual breakup date of river ice, while ARs closer to the breakup date have less impact.

16 **Abstract**

17 Atmospheric rivers (ARs) transport vast amounts of moisture from low to high lat-
 18 itude regions. One region particularly impacted by ARs is Interior Alaska (AK). We an-
 19alyze the impact of ARs on the annual river ice breakup date for 25 locations in AK. We
 20 investigate the AR-driven rise in local air temperatures and explore the relationship be-
 21 tween ARs and precipitation, including extremes and interannual variability. We found
 22 that AR events lead to an increase in local air temperatures for up to one week. Inter-
 23 annually, ARs account for 36% of total precipitation, explain 48% of precipitation vari-
 24 ability, and make up 57% of extreme precipitation events. By estimating the heat trans-
 25 fer between winter precipitation and the river ice surface, we conclude that heavy pre-
 26 cipitation events (HPEs) during the coldest period of the year delay river ice breakup
 27 dates, while HPEs occurring close to the breakup date have little impact on breakup tim-
 28 ing.

29 **Plain language summary**

30 Atmospheric rivers (ARs) are large storm systems originating in tropical regions
 31 capable of depositing large amounts of precipitation in high latitude regions. Using river
 32 ice breakup data recorded throughout Interior Alaska (AK) we set out to explore the re-
 33 lationship between ARs and annual river ice breakup timing from 1980 to 2023. We found
 34 that daily air temperature increases can last up to one week after an AR event. Inter-
 35 annually, ARs account for 36% of total precipitation, explain 48% of the variability of
 36 precipitation, and make up 57% of extreme precipitation events. We then calculated the
 37 total heat transfer between precipitation and the river ice surface. We used the mass and
 38 temperature of precipitation accumulated onto the river ice surface to approximate ther-
 39 mal energy exchange. The magnitude of energy exchange was then correlated to the river
 40 ice breakup timing. We found that heavy precipitation events (HPEs) from both local
 41 precipitation and ARs occurring relatively close to river ice breakup dates, have little cor-
 42 relation to the breakup date. However, HPEs that occur during the coldest period of the
 43 year (typically late December to early February) are strongly inversely correlated with
 44 river ice breakup timing and therefore delay the breakup date.

45 **1 Introduction**

46 Atmospheric rivers (ARs) are narrow corridors of intense water vapor transport that
 47 significantly influence hydrologic events, transporting most of the water vapor outside
 48 of the Tropics (American Meteorological Society, 2024). It is estimated that ARs are re-
 49 sponsible for as much as 90% of poleward water vapor transport at midlatitudes (Zhu
 50 & Newell, 1998). ARs contribute to extreme precipitation events across various regions
 51 worldwide (Espinoza et al., 2018; Massoud et al., 2019), including Western North Amer-
 52 ica (Dettinger et al., 2004; Neiman et al., 2008; Guan et al., 2010; Paul J. et al., 2011;
 53 Ralph et al., 2006; F. Martin et al., 2019; Dettinger et al., 2011) Europe (Lavers et al.,
 54 2013; Harald & Andreas, 2013), the Middle East (Massoud et al., 2020; Lashkari & Es-
 55 fandiari, 2020; Esfandiari & Shakiba, 2024), and Western South America (Viale et al.,
 56 2018). In recent years, the impacts of ARs on the cryosphere such as Greenland (Mattingly
 57 et al., 2018) and Antarctica (Gorodetskaya et al., 2014; Wille et al., 2021), have been
 58 more extensively analyzed.

59 In recent years, a growing number of works investigating the relationship between
 60 ARs and high latitude regions have been undertaken. Evidence shows that between 1981
 61 and 2020, higher atmospheric moisture content was significantly correlated with lower
 62 sea ice coverage over almost the entire Arctic Ocean (Li et al., 2022). For those same years,
 63 another analysis found that 100% of extreme temperature events in the Arctic (above
 64 0 °C) coincide with the presence of ARs (Ma et al., 2023). Analyses have noted a rela-

65 tionship between frequent AR activity and sea ice loss, caused by increased rainfall from
 66 moisture originating in lower latitudes (Zhang et al., 2023; Maclennan et al., 2022). How-
 67 ever Arctic systems are complicated, as the intense moisture transport within ARs can
 68 also result in heavy snowfall events, thus contributing to the accumulation of snowpack,
 69 especially in mountainous regions (Saavedra et al., 2020; Guan et al., 2010). Under the
 70 right conditions, this relationship has been found to actually increase the mass balance
 71 of glaciers (Little et al., 2019). (Little et al., 2019) found ARs to be the primary drivers
 72 of both highest ablation and snowfall events, substantially impacting glacier mass bal-
 73 ance at Brewster Glacier in New Zealand. Understanding the role of ARs in the cryosphere
 74 is essential for assessing their broader impact on regional water resources and glacier dy-
 75 namics in a changing climate.

76 While a number of works have explored the relationship between ARs and sea ice,
 77 glaciers, and ice sheets, to our knowledge there has been no study that investigates the
 78 relationship between ARs and Arctic river ice. Past studies have used physics based pro-
 79 cesses to model the annual breakup timing and conditions of Arctic river ice (Paily et
 80 al., 1974; Ashton, 1986; T. Prowse et al., 2007; Jasek, 1998; Shen, 2010). Through such
 81 studies, it is recognized that an increase in precipitation leads to an increase in stream-
 82 flow, altering the hydraulics associated with river ice breakup, and potentially acceler-
 83 ating mechanical breakup events (Ashton, 1986). It has also been proposed that increased
 84 snow pack as a result of increased precipitation contributes to breakup severity (T. D. Prowse
 85 & Beltaos, 2002). Using breakup records throughout Interior Alaska (AK) from the Alaska
 86 Pacific River Forecast Center Database (the same breakup records used in this analy-
 87 sis) Bieniek et al. (2011) determined that winter precipitation plays a relatively minor
 88 role in impacting the breakup timing of river ice and if anything accelerates the breakup
 89 timing as a result of increased streamflow. They also report that increased storm activ-
 90 ity in the spring leads to increased surface air temperature, leading to earlier breakup
 91 dates (Bieniek et al., 2011). However, their analysis used only 4 sites (as opposed to the
 92 25 used in this analysis) and aggregated precipitation seasonally, without accounting for
 93 the interaction between winter precipitation and temperature that occurs at a finer tem-
 94 poral resolution.

95 Our analysis aims to answer the following questions: 1.) Since ARs have been known
 96 to impact Arctic systems by increasing temperatures, is there a change in air temper-
 97 ature in different regions of AK corresponding to the presence of ARs? 2.) How do ARs
 98 contribute to precipitation throughout AK, considering how ARs impact total annual
 99 precipitation, interannual variability, and extreme events? 3.) How do ARs impact the
 100 timing of river ice breakup, does the presence of ARs accelerate or delay the timing of
 101 river ice breakup?

102 2 Data

103 2.1 Atmospheric Rivers Catalog

104 Similar to previous studies, we define ARs using integrated vapor transport (IVT)
 105 values constructed from 6-hourly values of 3-D wind and water vapor at eight pressure
 106 levels between 300 and 1,000 mb from the National Center for Environmental Protec-
 107 tion (NCEP) reanalysis data product (Kalnay et al., 1996). AR detection is based on
 108 version 3 of the tARget algorithm (Guan & Waliser, 2019; Guan, 2022). The IVT val-
 109 ues are calculated at the original resolution from the NCEP meteorological inputs (Saha
 110 et al., 2010). Guan and Waliser (2015) developed a global AR detection algorithm, which
 111 was updated and validated later with dropsonde data (Bin et al., 2018). This algorithm
 112 is employed in our study, which is based on a combination of IVT magnitude, direction,
 113 and geometry characteristics, to objectively identify ARs. Contiguous regions of enhanced
 114 IVT transport are first identified from magnitude thresholding (i.e., grid cells above the
 115 seasonally and locally dependent 85th percentile, or 100 $\frac{\text{kg}}{\text{m} \cdot \text{s}}$, whichever is greater) and

116 further filtered using directional and geometry criteria requirements. Although the $100 \frac{\text{kg}}{\text{m}^2\text{s}}$
 117 threshold is applied globally, it is intended for dry (including polar) regions since in other
 118 regions the 85th percentile is already larger than $100 \frac{\text{kg}}{\text{m}^2\text{s}}$. The detection algorithm was
 119 applied to NCEP reanalysis data at its native resolution of 2.5° . This detection algorithm
 120 had over 90% agreement in detecting AR landfall dates when compared with other AR
 121 detection methods for Western North America (Neiman et al., 2008), the United King-
 122 dom (Lavers et al., 2011), and East Antarctica (Gorodetskaya et al., 2014).

123 2.2 Daymet Daily Surface Weather and Climatological Summaries

124 Daily minimum (T_{\min}) and maximum (T_{\max}) temperatures and precipitation data
 125 were obtained from Daymet (M. Thornton et al., 2022). Daymet provides continuous and
 126 gridded estimates of daily weather at $1\text{km} \times 1\text{km}$ resolution. Daymet precipitation, T_{\min}
 127 and T_{\max} , were selected in this analysis due to their strong agreement with NCEP tem-
 128 perature time series for our region of interest (Figure 1C). Daymet is derived by inter-
 129 polating and extrapolating from in situ instruments and meteorological stations, and rep-
 130 resents a robust dataset for precipitation and temperature predictions across North Amer-
 131 ica (P. E. Thornton et al., 2021). This dataset has been a standard for validation among
 132 several analyses related to arctic regions (Diro & Sushama, 2019; Akinsanola et al., 2024).
 133 Figure 1 (A, B) show the annual mean precipitation and temperature for the year 2021
 134 across Alaska. For one of the study locations, Crooked Creek at the Kuskokwim River,
 135 Figure 1 (C) show the time series of precipitation, temperature and AR events for the
 136 year 2021.

137 2.3 River ice breakup observations

138 Observations for river ice breakup dates were obtained from the Alaska Pacific River
 139 Forecast Center database. While exact coordinates were unavailable, location coordinates
 140 were estimated based on proximity to weather stations and airports, to maintain spa-
 141 tial consistency with inputs used in Daymet's meteorological models. We identified 25
 142 locations (shown in Figure 1 (A, B)) in the database that had at least 35 breakup records
 143 between 1980 and 2023 (the current temporal availability of Daymet), although breakup
 144 records go as far back as 1896 for some locations. The 35 breakup records threshold was
 145 used because it allowed for the greatest number of locations with the most complete time
 146 series necessary for statistical analysis. There is always one breakup date per year, but
 147 not every year had a recorded date, so some years are represented as empty values in the
 148 dataset. On average, recorded break up dates range from mid-March to late-June This
 149 dataset has been used in several other studies such as (Murphy et al., 2022; Brown et
 150 al., 2018; Bieniek et al., 2011). As an example, the breakup date for Crooked Creek at
 151 the Kuskokwim River in 2021 occurred in early-May and is depicted in Figure 1C with
 152 a vertical purple dashed line.

153 3 Methods

154 To assess the influence of ARs on local temperature, we analyze the relationship
 155 between the presence of an AR and the temperature change at a specific location. The
 156 presence of an AR is represented numerically as a binary value indicating whether or not
 157 an AR is active on a particular date. We then estimate how many days this change in
 158 temperature persists. To do this, we conducted a pairwise *t*-test using varying tempo-
 159 ral window. In other words, for each AR occurrence in the dataset, a pre-AR time win-
 160 dows and post-AR time window each equal to n days in length was created before and
 161 after the AR event date, respectively, whereby: $n \in \{1, 2, 3, \dots, 14\}$. For values of n
 162 greater than one day the mean was calculated within each time window for T_{\min} and T_{\max} .
 163 These averaged temperatures were then calculated over all locations. Mean temperature
 164 pairs were assessed using a one tailed pairwise *t*-test to check whether ARs increased the

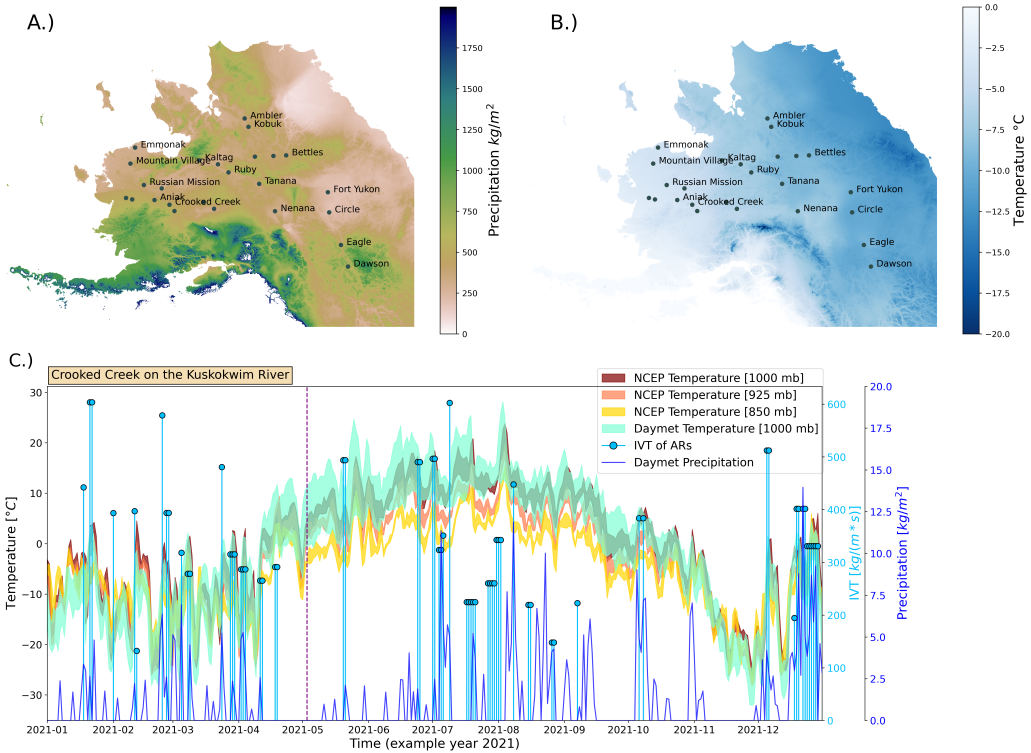


Figure 1. (A): map shows annual total precipitation for the year 2021. (B): map of average daily temperature for 2021. (C): One of the 25 locations (Crooked Creek on the Kuskokwim River) for the year 2021. Yellow, orange, red represent the temperature profiles (fill plot of $T_{\min} - T_{\max}$) from NCEP temperature data at 850, 925 and 1000mb respectively. Light green represents the Daymet temperature profile. Dark blue line shows precipitation from Daymet ($\frac{\text{kg}}{\text{m}^2}$) relative to the secondary y-axis in dark blue on the right. The light blue stem plots depict the IVT of AR events ($\frac{\text{kg}}{\text{m} \cdot \text{s}}$) relative to the secondary y-axis in light blue on the right. The vertical purple dashed line shows the breakup date for the Kuskokwim River in 2021 for Crooked Creek.

local temperature over period of time n ($\alpha = 0.05$). For example, if $n = 3$ assessing T_{\min} , then the mean of T_{\min} three days prior to each AR event will be compared to the mean of T_{\min} for the three days post each AR event.

We explored AR contribution to precipitation by separating precipitation events occurring on days with an active AR. We then used the Wilcoxon rank-sum test (Rey & Neuhauser, 2011) to test the hypothesis that AR events tend to produce more precipitation than other precipitation events. We opted to use a non-parametric test (Wilcoxon rank-sum test) because the distributions of precipitation were shown to not be normal after log transformation using the Shapiro-Wilks test (Shapiro & Wilk, 1965). We also estimated the interannual variability of precipitation associated with ARs by conducting a univariate ordinary least squares regression (OLS). For extremes, we extracted the top 5% of precipitation events and determined what fraction of those events occurred on days with active AR event.

To determine the impact that ARs have on river ice breakup timing, we estimate the heat transfer between the river ice and the precipitation accumulating on the surface. Assuming presence of frozen layer of ice on river surface, we estimate the sensible heat transfer between river surface and incoming precipitation using Equation 1. Latent heat transfer fluxes were assumed to be relatively small and thus ignored in our simplified heat transfer calculations.

$$q_t = \rho \cdot m \cdot \Delta T \quad (1)$$

where q_t is heat flux ($\frac{\text{J}}{\text{m}^2}$) at a given day t ; ρ the specific heat of the precipitation (assumed to be either water or snow depending on the temperature) ($\frac{\text{J}}{\text{kg}\cdot\text{C}}$); ΔT is the difference between the temperature of the precipitation which is approximated using T_{\min} as a proxy, and the river ice surface which is assumed to be at 0°C ; m the mass of the precipitation per unit area ($\frac{\text{kg}}{\text{m}^2}$).

Heat transfer fluxes were calculated as a daily series for a period of six months prior to the breakup date. Time of occurrence and thermal conditions associated with precipitation events during winter and spring have differential impacts to reinforce vs weaken the river ice layer and thus the date of the breakup. We fit a temporal bias function (Equation 2), a double exponential function, applied to the heat transfer equation to assess the days of the year when precipitation events were more impactful on breakup timing. Bias function is a symmetric unimodal exponential function to help identify the most influential precipitation time period determining the annual time of river ice break up. Bias function was fit individually for each of the study locations.

$$f(t; \gamma, \kappa, DOY, c) = \begin{cases} \frac{e^{-\gamma \cdot (-t - DOY)} - 1}{e^{-\gamma \cdot (t - DOY)} - 1} & \text{if } t < c \\ \frac{\kappa}{\kappa} & \text{if } t \geq c \end{cases} \quad (2)$$

where γ is a scale parameter impacting the width of the exponential function; t is time in days; DOY is the Gregorian day of year that the breakup date occurred; c is a location parameter dictating the center placement of the function; κ is a normalizing constant. Finally, Equation 3 solves for $Q_{\text{year}, \text{location}}$, the total thermal energy exchange for a given location, for a given breakup year. Equation 3 is tuned over the entire hyper-parameter search space for each location and each breakup year, optimized by selecting the parameter values that produce the Pearson correlation coefficient with the greatest absolute value. Here i is the starting day of the time series approximately six months prior to the breakup date.

$$Q_{\text{year, location}} = \sum_{t=i}^{t=DOY} f(t; \gamma, \kappa, DOY, c) \cdot q_t \quad (3)$$

207 **4 Results**

208 **4.1 Atmospheric rivers impact on temperature**

209 We applied the pairwise t -test comparing pre-AR and post-AR time windows of
 210 length n at all locations. Figures 2A and 2B show the change in p -values for each value
 211 of n where the dashed lines represent the mean p -value across the study locations and
 212 the filled color curved signifies the interquartile range (IQR). Figure 2C and 2D shows
 213 the mean increase in temperature from the pre-AR time window to the post-AR time
 214 window for varying time window sizes n . Analysis shows an increase in air temperature
 215 during period following an AR event, with mean temperature increases higher for T_{\min}
 216 compared to T_{\max} , with the difference receding over longer time windows. The temper-
 217 ature differences were statistically significant for T_{\min} (based on an $\alpha = 0.05$) for up
 218 temporal windows of 8 days after an AR event. The increase in daily minimum temper-
 219 ature can be as high as 1.5 °C ($n = 2$) (Figure 2C). For T_{\max} , the differences were sta-
 220 tistically significant for up to 6 days after an AR event (Figure 2B) with an increase as
 221 high as 0.75 °C ($n = 3, 4$) (Figure 2D). These statistically significant temperature in-
 222 crease following AR events were true at all locations in our study, represented by the Fig-
 223 ure 2A fill plot.

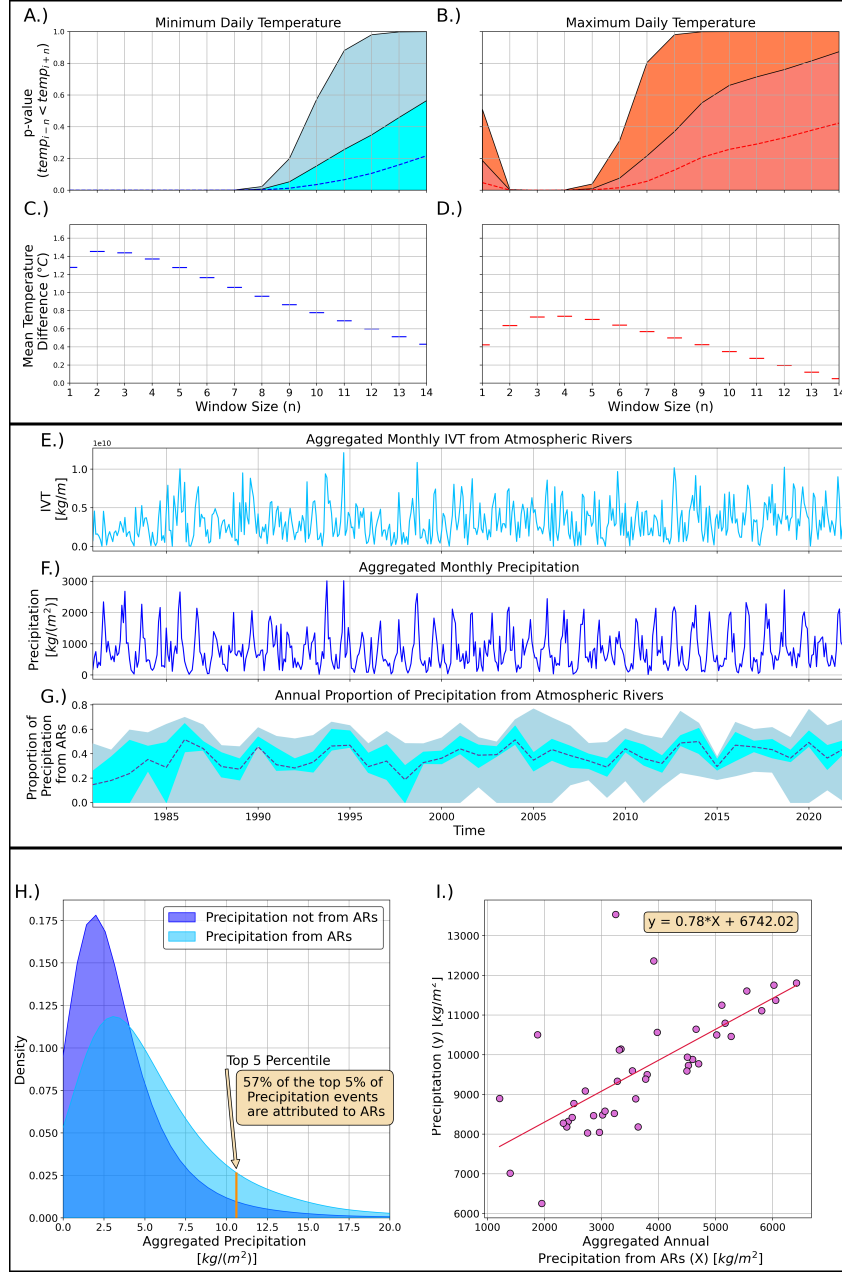


Figure 2. (A and B): p -values from the paired t -test given time window size (n) surrounding the AR event date (A: T_{\min} ; B: T_{\max}). Dashed line represent the mean, while the filled color curves show interquartile range (25th and 75th percentile); (C and D): mean increase in temperature ($^{\circ}\text{C}$) accompanying each AR, calculated between the pre-AR time window and the post-AR time window (C: T_{\min} ; D: T_{\max}). (E): time series of IVT $\frac{\text{kg}}{\text{m}}$ aggregated monthly over all locations. (F): time series of total precipitation $\frac{\text{kg}}{\text{m}^2}$ aggregated monthly over all study locations. (G): proportion of precipitation accounted for by ARs on an annual basis. (H): kernel density plots showing the distribution of local precipitation (dark blue) and precipitation from ARs (light blue). (I): ordinary least squares regression plot using total annual precipitation from ARs, to predict total annual precipitation.

224 **4.2 Atmospheric rivers impact on precipitation**

225 Figures 2E and 2F show the monthly IVT from AR events and monthly total pre-
 226 cipitation through the span of the data record, aggregated over all locations, respectively.
 227 Figure 2G shows the proportion of total annual precipitation occurring on days with ac-
 228 tive ARs over time, where light blue depicts the IQR of proportions and blue-grey rep-
 229 resents proportions outside of the IQR, across all 25 locations. The dashed line repre-
 230 sents the mean proportion. ARs tend to account for 36% of precipitation on average (Fig-
 231 ure 2G), with a high degree of variability across years and locations. In 2005 and 2020
 232 for example, nearly 80% of the total precipitation at some locations occurred on days with
 233 active AR events. The results from the Wilcoxon rank-sum test show that precipitation
 234 during active ARs tends to be greater in magnitude than non-AR precipitation (test statistic =
 235 -83.85 ; p-value ≈ 0.0). In addition, we found that of the top 5% of high precipitation
 236 events (HPEs), 57% occurred during active ARs (Figure 2H). Correlating total precip-
 237 itation from AR days, to total annual precipitation using a univariate OLS, we find that
 238 the coefficient of determination (R^2) is equal to 0.48 (Figure 2I). This indicates that ARs
 239 explain about 48% of interannual variability in precipitation, across all 25 locations.

240 **4.3 Transfer of energy based on Precipitation**

241 To estimate the impact HPEs precipitation events have on river ice breakup dates,
 242 we use Equation 3 to estimate the heat transfer between precipitation and the river ice
 243 surface. Equation 3 was solved using double exponential bias function to temporally-weigh
 244 events of higher influence (Figures 3A, B, C), and using uniform weights as baseline for
 245 comparison (Figures 3D, E, F). When using a temporal bias function, the relationship
 246 between integrated heat transfer due to precipitation and time of river ice break up were
 247 identified with strong correlation (Pearson correlation coefficient (r_p) = -0.84 and a Spear-
 248 man correlation coefficient (r_s) = -0.80 at Crooked Creek on the Kuskokwim river (Fig-
 249 ure 3A)). In contrast, very weak correlations were identified when fitting the relation-
 250 ship using temporally uniform weights (Figure 3B), thus highlighting the need for tem-
 251 poral bias function. This exercise allows us to determine whether or not that integrated
 252 energy accelerates or decelerates the breakup of river ice. We performed the analysis for
 253 all precipitation events, and also by separating the precipitation time series into days with
 254 and without AR events. We find that there is a strong negative correlation between the
 255 heat transfer and the DOY on which the river ice break up occurs (Figure 3A). In this
 256 context, negative values along the y-axis of Figures 3A and 3D are interpreted as a neg-
 257 ative heat exchange, suggesting a net cooling effect on the river ice surface as the pre-
 258 cipitation below freezing temperature are accumulated on the river ice surface. ~~This is~~
 259 ~~optimized for when the temporally weighted bias curve is positioned during the coldest~~
 260 ~~period of the year – typically between late November and early February (Figure 3C).~~
 261 **THIS NEEDS REWORDING** Peak of the temporally-weighted bias curve are typically
 262 located during the coldest period of the year, typically between late November and early
 263 February (Figure 3C). In other words, the presence high magnitude precipitation events,
 264 occurring on colder days of the year, show a strong inverse correlation to the time of breakup.
 265 For example (3), Crooked Creek on the Kuskokwim River has a clear negative trend, with
 266 cooling effect of precipitation on the river ice surface, delays the DOY of the break up.
 267 Frequency of AR events that occurred during period of six months prior to the breakup
 268 date by itself was insufficient predictor (Figures 3B, E) of the break up date.



269 While Figure 3 focuses on single selected site, Table 1 shows the correlation for each
 270 location, after tuning parameters c and γ are optimized and applied to Equation 3 in-
 271 dividually at each location. Table 1 also shows the center of the bias curve c (month-
 272 day) that was selected for, at each location, given the integrand for precipitation used
 273 in Equation 3 (ie. Total Precipitation, Precipitation from ARs, Precipitation not from
 274 ARs).

Crooked Creek on the Kuskokwim River

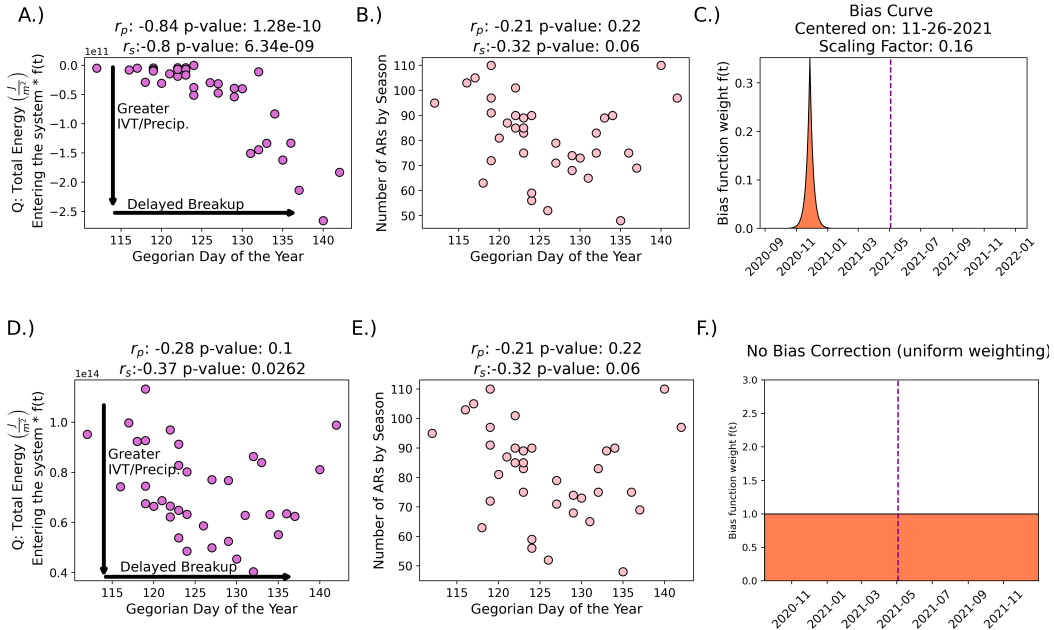


Figure 3. top row: (A): scatter plot between thermal energy transfer for all precipitation events and *DOY* (the Gregorian day of year that the breakup date occurred); (B): scatter plot of the number of ARs that occurred in the six months prior to the breakup date and *DOY*; (C): temporal bias curve for the year 2021 with the breakup date represented by the vertical dashed line. bottom row: same as the top row except depicting the results when a temporal bias is not utilized.

275 5 Conclusion and Discussion

276 This study investigated the impact atmospheric rivers (ARs) and **heavy precipitation events (HPEs)** have on the timing of river ice breakup across site in Alaska. We
 277 explored the impact of ARs on local temperature increases throughout the study domain,
 278 the contribution of ARs to precipitation events, including variability and extremes, and
 279 determined the impact of ARs and HPEs on the *DOY* on which the ice on the surface
 280 of Alaskan rivers eventually breaks.

282 We found that ARs generally lead to up to a week-long persistent increase in daily
 283 temperature (minimum and maximum) across Alaska, with temperatures rising by as
 284 much as 1.5°C for T_{\min} and 0.75°C for T_{\max} . These findings are consistent with many
 285 past studies that have shown that warm moisture brought on by ARs can warm the cryosphere
 286 (Wille et al., 2021; Ma et al., 2023; Li et al., 2022; Zhang et al., 2023). Our analysis
 287 also show that ARs account for a significant portion of total annual precipitation in Alaska,
 288 contributing to 36% of total precipitation by volume on average. They also explain 48%
 289 of interannual variability and lead to 57% of extreme precipitation events (precipitation
 290 events within the top 5% of deposition). These results are consistent with past works,
 291 such as Nash et al. (2024) which showed that throughout Southeast Alaska as few as six
 292 annual AR events can account for 68% - 91% of precipitation days. Our analysis show
 293 evidence that intense ARs occurring during the coldest period of the year appear to de-
 294 lay the annual breakup date of river ice. Our results do not show that ARs are unique
 295 relative to local forms of precipitation in this regard (Table 1), with no evidence that in-

296 creased precipitation events of any kind closer to the breakup date accelerates the breakup
 297 date. This is likely attributed to a combination of the heat transfer from precipitation,
 298 as well as changes in the river ice surface as a result of snowfall. Increased snow accu-
 299 mulation increase the albedo of the river surface, as well as provide thermal insulation,
 300 mitigating the effects of temperature fluctuations during the coldest period of the year.
 301 It should be noted that a limitation of our analysis is the assumption that the river ice
 302 surface temperature is held constant at 0°C and that air temperature is a reasonable proxy
 303 for incoming precipitation. We were unable to find a complete dataset on river ice sur-
 304 face temperatures for the locations and time period of our study. Thus, we assume that
 305 the mass of liquid, snow or ice deposited on the river surface, times its temperature, will
 306 be a sufficient approximate indicator of the heat exchanged in the system – a process
 307 that becomes far more difficult to model when the structure of accumulated snow is
 308 taken into consideration near 0°C.



309 Understanding the influence of ARs and other HPEs on the timing of river ice break-
 310 up in Alaska is crucial for predicting and managing the impacts of climate change in the
 311 region, especially since studies have shown that AR frequency and intensity in this re-
 312 gion are expected to increase in a warmer world (Espinoza et al., 2018; Massoud et al.,
 313 2019). The findings of our suggest that ARs have significant influence on the climate and
 314 terrestrial hydrology across Alaska, affecting temperature, precipitation, and river ice
 315 dynamics. Further research in this area could help improve our understanding of ARs
 316 and their role in shaping the climate of high-latitude regions.

317 Data Availability Statement

318 Daily Daymet precipitation and temperature data is available through the Oak Ridge
 319 National Laboratory Distributed Active Archive at [https://daymet.ornl.gov/single](https://daymet.ornl.gov/single-pixel/)
 320 -pixel/. The National Center for Environmental Protection temperature data can found
 321 at <https://psl.noaa.gov/data/index.html>. River ice breakup records are maintained
 322 by the Alaska Pacific River Forecast Center at <https://www.weather.gov/aprfc/breakupMap>.
 323 The AR database (<https://doi.org/10.25346/S6/Y0150N>) is available via the Global
 324 Atmospheric Rivers DataVerse at <https://dataverse.ucla.edu/dataverse/ar>. NCEP-
 325 NCAR Reanalysis 1 data were obtained from the NOAA Physical Sciences Laboratory,
 326 Boulder, Colorado, USA, <https://psl.noaa.gov>. WE SHOULD INCLUDE A GITHUB
 327 LINK/DOI OF CODES USED IN THIS STUDY.

328 Acknowledgments

329 This work was supported by the U.S. Department of Energy, Office of Science, Biolog-
 330 ical and Environmental Research (BER) Regional and Global Model Analysis (RGMA)
 331 program, as part of The Interdisciplinary Research for Arctic Coastal Environments (In-
 332 teRFACE) project. Development of the AR database was supported by NASA and the
 333 California Department of Water Resources. This manuscript has been authored in part
 334 by UT-Battelle, LLC, under contract DE-AC05-00OR22725 with the US Department
 335 of Energy (DOE). The publisher acknowledges the US government license to provide pub-
 336 lic access under the DOE Public Access Plan (<http://energy.gov/downloads/doe-public-access-plan>).
 337

338 References

- 339 Akinsanola, A. A., Jung, C., Wang, J., & Kotamarthi, V. R. (2024). Evaluation
 340 of precipitation across the contiguous united states, alaska, and puerto rico in
 341 multi-decadal convection-permitting simulations. *Scientific Reports*, 14(1),
 342 1238. Retrieved from <https://doi.org/10.1038/s41598-024-51714-3> doi:
 343 10.1038/s41598-024-51714-3

- 344 American Meteorological Society. (2024). *Glossary of meteorology: Atmospheric*
 345 *river.* Retrieved from https://glossary.ametsoc.org/wiki/Atmospheric_river?_cf_chl_tk=LTK3vMN1WxxKfhHCGpS05IMiQaNMnEAledLyvfTD7T0-1717350416-0.0.1.1-4330 (Accessed: 2024-06-03)
- 348 Ashton, G. (1986). *River and lake ice engineering.* Water Resources Publications.
 349 Retrieved from <https://books.google.com/books?id=xg1YVjAsnt8C>
- 350 Bieniek, P. A., Bhatt, U. S., Rundquist, L. A., Lindsey, S. D., Zhang, X., &
 351 Thoman, R. L. (2011). Large-scale climate controls of interior alaska river
 352 ice breakup. *Journal of Climate*, 24(1), 286 - 297. Retrieved from <https://journals.ametsoc.org/view/journals/clim/24/1/2010jcli3809.1.xml>
 353 doi: 10.1175/2010JCLI3809.1
- 355 Bin, G., Duane E., W., & F. Martin, R. (2018). An intercomparison between re-
 356 analysis and dropsonde observations of the total water vapor transport in
 357 individual atmospheric rivers. *Journal of Hydrometeorology*, 19(2), 321 - 337.
 358 Retrieved from https://journals.ametsoc.org/view/journals/hydr/19/2/jhm-d-17-0114_1.xml doi: 10.1175/JHM-D-17-0114.1
- 360 Brown, D. R. N., Brinkman, T. J., Verbyla, D. L., Brown, C. L., Cold, H. S., &
 361 Hollingsworth, T. N. (2018). Changing river ice seasonality and impacts on
 362 interior alaskan communities. *Weather, Climate, and Society*, 10(4), 625 - 640.
 363 Retrieved from https://journals.ametsoc.org/view/journals/wcas/10/4/wcas-d-17-0101_1.xml doi: 10.1175/WCAS-D-17-0101.1
- 365 Dettinger, M. D., Cayan, D. R., Meyer, M. K., & Jeton, A. E. (2004). Simulated
 366 hydrologic responses to climate variations and change in the merced, carson,
 367 and american river basins, sierra nevada, california, 1900–2099. *Climatic*
 368 *Change*, 62(1), 283–317. Retrieved from <https://doi.org/10.1023/B:CLIM.0000013683.13346.4f>
- 370 Dettinger, M. D., Ralph, F. M., Das, T., Neiman, P. J., & Cayan, D. R. (2011).
 371 Atmospheric rivers, floods and the water resources of california. *Water*, 3(2),
 372 445–478. Retrieved from <https://www.mdpi.com/2073-4441/3/2/445> doi:
 373 10.3390/w3020445
- 374 Diro, G. T., & Sushama, L. (2019). Simulating canadian arctic climate at
 375 convection-permitting resolution. *Atmosphere*, 10(8). Retrieved from
 376 <https://www.mdpi.com/2073-4433/10/8/430> doi: 10.3390/atmos10080430
- 377 Esfandiari, N., & Shakiba, A. (2024). The extraordinary atmospheric rivers
 378 analysis over the middle east: Large-scale drivers, structure, effective
 379 sources, and precipitation characterization. *Dynamics of Atmospheres and*
 380 *Oceans*, 105, 101430. Retrieved from <https://www.sciencedirect.com/science/article/pii/S0377026523000817> doi: <https://doi.org/10.1016/j.dynatmoce.2023.101430>
- 383 Espinoza, V., Waliser, D. E., Guan, B., Lavers, D. A., & Ralph, F. M. (2018).
 384 Global analysis of climate change projection effects on atmospheric rivers.
 385 *Geophysical Research Letters*, 45(9), 4299-4308. Retrieved from <https://agupubs.onlinelibrary.wiley.com/doi/abs/10.1029/2017GL076968> doi:
 386 <https://doi.org/10.1029/2017GL076968>
- 388 F. Martin, R., Jonathan J., R., Jason M., C., Michael, D., Michael, A., David, R.,
 389 ... Chris, S. (2019). A scale to characterize the strength and impacts of atmo-
 390 spheric rivers. *Bulletin of the American Meteorological Society*, 100(2), 269 -
 391 289. Retrieved from <https://journals.ametsoc.org/view/journals/bams/100/2/bams-d-18-0023.1.xml> doi: 10.1175/BAMS-D-18-0023.1
- 393 Gorodetskaya, I. V., Tsukernik, M., Claes, K., Ralph, M. F., Neff, W. D., &
 394 Van Lipzig, N. P. M. (2014). The role of atmospheric rivers in anomalous snow
 395 accumulation in east antarctica. *Geophysical Research Letters*, 41(17), 6199-
 396 6206. Retrieved from <https://agupubs.onlinelibrary.wiley.com/doi/abs/10.1002/2014GL060881> doi: <https://doi.org/10.1002/2014GL060881>
- 398 Guan, B. (2022). [Data] *Global Atmospheric Rivers Database, Version 3.* UCLA

- 399 Dataverse. Retrieved from <https://doi.org/10.25346/S6/Y015ON> doi: 10
 400 .25346/S6/Y015ON
- 401 Guan, B., Molotch, N. P., Waliser, D. E., Fetzer, E. J., & Neiman, P. J. (2010).
 402 Extreme snowfall events linked to atmospheric rivers and surface air tem-
 403 perature via satellite measurements. *Geophysical Research Letters*, 37(20).
 404 Retrieved from <https://agupubs.onlinelibrary.wiley.com/doi/abs/10.1029/2010GL044696>
 405 doi: <https://doi.org/10.1029/2010GL044696>
- 406 Guan, B., & Waliser, D. (2019, 12). Tracking atmospheric rivers globally: Spa-
 407 tial distributions and temporal evolution of life cycle characteristics. *Journal of*
 408 *Geophysical Research: Atmospheres*, 124. doi: 10.1029/2019JD031205
- 409 Guan, B., & Waliser, D. E. (2015). Detection of atmospheric rivers: Evaluation
 410 and application of an algorithm for global studies. *Journal of Geophysical Re-*
 411 *search: Atmospheres*, 120(24), 12514-12535. Retrieved from <https://agupubs.onlinelibrary.wiley.com/doi/abs/10.1002/2015JD024257> doi: <https://doi.org/10.1002/2015JD024257>
- 412 Harald, S., & Andreas, S. (2013). Moisture origin and meridional trans-
 413 port in atmospheric rivers and their association with multiple cyclones.
 414 *Monthly Weather Review*, 141(8), 2850 - 2868. Retrieved from <https://journals.ametsoc.org/view/journals/mwre/141/8/mwr-d-12-00256.1.xml>
 415 doi: 10.1175/MWR-D-12-00256.1
- 416 Jasek, M. (1998, July 27–31). 1998 break-up and flood on the yukon river at dawson
 417 – did el niño and climate change play a role? In H. Shen (Ed.), *Ice in surface*
 418 *waters: Proceedings of the 14th international symposium on ice* (pp. 761–768).
 419 Rotterdam: A.A. Balkema.
- 420 Kalnay, E., Kanamitsu, M., Kistler, R., Collins, W., Deaven, D., Gandin, L., ...
 421 Joseph, D. (1996). The ncep/ncar 40-year reanalysis project. *Bulletin*
 422 *of the American Meteorological Society*, 77(3), 437 - 472. Retrieved from
 423 [https://journals.ametsoc.org/view/journals/bams/77/3/1520-0477_1996_077_0437_tnyrp_2.0.co_2.xml](https://journals.ametsoc.org/view/journals/bams/77/3/1520-0477_1996_077_0437_tnyrp_2.0_co_2.xml) doi: 10.1175/1520-0477(1996)077(0437: TNYRP)2.0.CO;2
- 424 Lashkari, H., & Esfandiari, N. (2020, 05). Identifying atmospheric river events and
 425 their paths into iran. *Theoretical and Applied Climatology*, 140. doi: 10.1007/
 426 s00704-020-03148-w
- 427 Lavers, D. A., Allan, R. P., Villarini, G., Lloyd-Hughes, B., Brayshaw, D. J., &
 428 Wade, A. J. (2013). Future changes in atmospheric rivers and their impli-
 429 cations for winter flooding in britain. *Environmental Research Letters*, 8(3).
 430 Retrieved from <https://doi.org/10.1088/1748-9326/8/3/034010> doi:
 431 10.1088/1748-9326/8/3/034010
- 432 Lavers, D. A., Allan, R. P., Wood, E. F., Villarini, G., Brayshaw, D. J., & Wade,
 433 A. J. (2011). Winter floods in britain are connected to atmospheric
 434 rivers. *Geophysical Research Letters*, 38(23). Retrieved from <https://agupubs.onlinelibrary.wiley.com/doi/abs/10.1029/2011GL049783> doi:
 435 <https://doi.org/10.1029/2011GL049783>
- 436 Li, L., Cannon, F., Mazloff, M. R., Subramanian, A. C., Wilson, A. M., & Ralph,
 437 F. M. (2022). Impact of atmospheric rivers on arctic sea ice variations. *EGU-*
 438 *sphere*, 2022, 1–21. Retrieved from <https://egusphere.copernicus.org/preprints/2022/egusphere-2022-36/> doi: 10.5194/egusphere-2022-36
- 439 Little, K., Kingston, D. G., Cullen, N. J., & Gibson, P. B. (2019). The role of at-
 440 mospheric rivers for extreme ablation and snowfall events in the southern alps
 441 of new zealand. *Geophysical Research Letters*, 46(5), 2761-2771. Retrieved
 442 from <https://agupubs.onlinelibrary.wiley.com/doi/abs/10.1029/2018GL081669> doi: <https://doi.org/10.1029/2018GL081669>
- 443 Ma, W., Wang, H., Chen, G., Qian, Y., Baxter, I., Huo, Y., & Seefeldt, M. W.
 444 (2023). Wintertime extreme warming events in the high arctic: Characteristics,
 445 drivers, trends, and the role of atmospheric rivers. *EGUsphere*. Retrieved
 446

- 454 from <https://doi.org/10.5194/egusphere-2023-2018> (Preprint) doi:
 455 10.5194/egusphere-2023-2018
- 456 Maclennan, M. L., Lenaerts, J. T. M., Shields, C., & Wille, J. D. (2022). Contribution
 457 of atmospheric rivers to antarctic precipitation. *Geophysical Research Letters*, 49(18). Retrieved 2024-04-16, from <https://onlinelibrary.wiley.com/doi/abs/10.1029/2022GL100585> doi: 10.1029/2022GL100585
- 460 Massoud, E., Espinoza, V., Guan, B., & Waliser, D. (2019). Global cli-
 461 mate model ensemble approaches for future projections of atmospheric
 462 rivers. *Earth's Future*, 7(10), 1136-1151. Retrieved from <https://agupubs.onlinelibrary.wiley.com/doi/abs/10.1029/2019EF001249> doi:
 463 <https://doi.org/10.1029/2019EF001249>
- 465 Massoud, E., Massoud, T., Guan, B., Sengupta, A., Espinoza, V., De Luna,
 466 M., ... Waliser, D. (2020). Atmospheric rivers and precipitation in the
 467 middle east and north africa (mena). *Water*, 12(10). Retrieved from
 468 <https://www.mdpi.com/2073-4441/12/10/2863> doi: 10.3390/w12102863
- 469 Mattingly, K. S., Mote, T. L., & Fettweis, X. (2018). Atmospheric river im-
 470 pacts on greenland ice sheet surface mass balance. *Journal of Geophysi-
 471 cal Research: Atmospheres*, 123(16), 8538-8560. Retrieved from <https://agupubs.onlinelibrary.wiley.com/doi/abs/10.1029/2018JD028714> doi:
 472 <https://doi.org/10.1029/2018JD028714>
- 474 Murphy, J. M., Garcia, S., Piston, A., Moss, J. H., Howard, K., Fergusson, E. A.,
 475 ... others (2022). Coastal surveys in alaska and their application to salmon
 476 run-size and harvest forecasts. *North Pacific Anadromous Fish Commission
 477 Technical Report*(18).
- 478 Nash, D., Rutz, J. J., & Jacobs, A. (2024). Atmospheric rivers in southeast alaska:
 479 Meteorological conditions associated with extreme precipitation. *Journal
 480 of Geophysical Research: Atmospheres*, 129(4), e2023JD039294. Retrieved
 481 from <https://agupubs.onlinelibrary.wiley.com/doi/abs/10.1029/2023JD039294> (e2023JD039294 2023JD039294) doi: <https://doi.org/10.1029/2023JD039294>
- 484 Neiman, P. J., Ralph, F. M., Wick, G. A., Kuo, Y.-H., Wee, T.-K., Ma, Z., ... Det-
 485 ttinger, M. D. (2008). Diagnosis of an intense atmospheric river impacting
 486 the pacific northwest: Storm summary and offshore vertical structure observed
 487 with cosmic satellite retrievals. *Monthly Weather Review*, 136(11), 4398 -
 488 4420. Retrieved from <https://journals.ametsoc.org/view/journals/mwre/136/11/2008mwr2550.1.xml> doi: 10.1175/2008MWR2550.1
- 490 Paily, P., Macagno, E., & Kennedy, J. (1974, 3). Winter-regime surface heat loss
 491 from heated streams. research report. *US Office of Scientific and Technical In-
 492 formation*. Retrieved from <https://www.osti.gov/biblio/7179276>
- 493 Paul J., N., Lawrence J., S., F. Martin, R., Mimi, H., & Gary A., W. (2011).
 494 Flooding in western washington: The connection to atmospheric rivers.
 495 *Journal of Hydrometeorology*, 12(6), 1337 - 1358. Retrieved from <https://journals.ametsoc.org/view/journals/hydr/12/6/2011jh1358.1.xml> doi:
 496 10.1175/2011JHM1358.1
- 498 Prowse, T., Bonsal, B., Duguay, C., & Lacroix, M. (2007). River-ice break-up/freeze-
 499 up: a review of climatic drivers, historical trends and future predictions. *An-
 500 nals of Glaciology*, 46, 443-451. doi: 10.3189/172756407782871431
- 501 Prowse, T. D., & Beltaos, S. (2002). Climatic control of river-ice hydrology: a review.
 502 *Hydrological Processes*, 16(4), 805-822. Retrieved from
 503 <https://onlinelibrary.wiley.com/doi/abs/10.1002/hyp.369> doi:
 504 <https://doi.org/10.1002/hyp.369>
- 505 Ralph, F. M., Neiman, P. J., Wick, G. A., Gutman, S. I., Dettinger, M. D., Cayan,
 506 D. R., & White, A. B. (2006). Flooding on california's russian river: Role
 507 of atmospheric rivers. *Geophysical Research Letters*, 33(13). Retrieved
 508 from <https://agupubs.onlinelibrary.wiley.com/doi/abs/10.1029/>

- 509 2006GL026689 doi: <https://doi.org/10.1029/2006GL026689>
- 510 Rey, D., & Neuhauser, M. (2011). Wilcoxon-signed-rank test. In M. Lovric (Ed.), *International encyclopedia of statistical science* (pp. 1658–1659). Berlin, Heidelberg: Springer Berlin Heidelberg. Retrieved from https://doi.org/10.1007/978-3-642-04898-2_616 doi: 10.1007/978-3-642-04898-2_616
- 511 Saavedra, F., Cortés, G., Viale, M., Margulis, S., & McPhee, J. (2020). Atmospheric rivers contribution to the snow accumulation over the southern
512 andes (26.5° s–37.5° s). *Frontiers in Earth Science*, 8. Retrieved from
513 <https://www.frontiersin.org/articles/10.3389/feart.2020.00261>
514 doi: 10.3389/feart.2020.00261
- 515 Saha, S., Moorthi, S., Pan, H.-L., Wu, X., Wang, J., Nadiga, S., ... Goldberg, M.
516 (2010). The ncep climate forecast system reanalysis. *Bulletin of the American
517 Meteorological Society*, 91(8), 1015 - 1058. Retrieved from https://journals.ametsoc.org/view/journals/bams/91/8/2010bams3001_1.xml
518 doi: 10.1175/2010BAMS3001.1
- 519 Shapiro, S. S., & Wilk, M. B. (1965). An analysis of variance test for normality
520 (complete samples). *Biometrika*, 52(3-4), 591–611.
- 521 Shen, H. T. (2010). Mathematical modeling of river ice processes. *Cold Regions
522 Science and Technology*, 62(1), 3-13. Retrieved from <https://www.sciencedirect.com/science/article/pii/S0165232X10000339> doi:
523 <https://doi.org/10.1016/j.coldregions.2010.02.007>
- 524 Thornton, M., Shrestha, R., Wei, Y., Thornton, P., Kao, S.-C., & Wilson, B.
525 (2022). *Daymet: Annual climate summaries on a 1-km grid for north america,
526 version 4 r1*. ORNL Distributed Active Archive Center. Retrieved
527 from https://daac.ornl.gov/cgi-bin/dsviewer.pl?ds_id=2130 doi:
528 10.3334/ORNLDAAAC/2130
- 529 Thornton, P. E., Shrestha, R., Thornton, M., Kao, S.-C., Wei, Y., & Wilson,
530 B. E. (2021, 7 23). Gridded daily weather data for north america with
531 comprehensive uncertainty quantification. *Scientific Data*, 8(1), 190. Re-
532 tried from <https://doi.org/10.1038/s41597-021-00973-0> doi:
533 10.1038/s41597-021-00973-0
- 534 Viale, M., Valenzuela, R., Garreaud, R. D., & Ralph, F. M. (2018). Impacts
535 of atmospheric rivers on precipitation in southern south america. *Journal
536 of Hydrometeorology*, 19(10), 1671 - 1687. Retrieved from https://journals.ametsoc.org/view/journals/hydr/19/10/jhm-d-18-0006_1.xml
537 doi: 10.1175/JHM-D-18-0006.1
- 538 Wille, J. D., Favier, V., Gorodetskaya, I. V., Agosta, C., Kittel, C., Beeman, J. C.,
539 ... Codron, F. (2021). Antarctic atmospheric river climatology and pre-
540 cipitation impacts. *Journal of Geophysical Research: Atmospheres*, 126(8),
541 e2020JD033788. Retrieved from <https://agupubs.onlinelibrary.wiley.com/doi/abs/10.1029/2020JD033788> (e2020JD033788 2020JD033788) doi:
542 <https://doi.org/10.1029/2020JD033788>
- 543 Zhang, P., Chen, G., Ting, M., Ruby Leung, L., Guan, B., & Li, L. (2023, March).
544 More frequent atmospheric rivers slow the seasonal recovery of arctic sea ice.
545 *Nature Climate Change*, 13(3), 266–273. Retrieved from <https://doi.org/10.1038/s41558-023-01599-3> doi: 10.1038/s41558-023-01599-3
- 546 Zhu, Y., & Newell, R. E. (1998). A proposed algorithm for moisture fluxes
547 from atmospheric rivers. *Monthly Weather Review*, 126(3), 725 - 735.
548 Retrieved from https://journals.ametsoc.org/view/journals/mwre/126/3/1520-0493_1998_126_0725_apafmf_2.0.co_2.xml doi: 10.1175/1520-0493(1998)126(0725:APAFMF)2.0.CO;2

560 **Appendix A.**

Table 1. Table showing the Pearson correlation coefficients between the total thermal energy exchange (Q) as derived by Equation 3, assuming an exponential temporal bias (Equation 2), and the day of the year the breakup occurred (DOY), by location. The optimal center placement of the temporal bias (month-day) is also provided [r_p |center date of bias]

Location	Total Precipitation	Precipitation from ARs	Precipitation not from ARs
Akiak Kuskokwim River	-0.78 11-12	-0.78 2-5	-0.80 1-15
Allakaket Koyukuk River	-0.81 12-10	-0.69 10-23	-0.80 12-3
Ambler Kobuk River	-0.84 2-5	-0.67 2-5	-0.83 2-12
Aniak Kuskokwim River	-0.80 11-19	-0.81 1-29	-0.77 11-12
Bethel Kuskokwim River	-0.72 12-3	-0.75 2-5	-0.73 12-10
Bettles Koyukuk River	-0.79 2-19	-0.70 10-23	-0.81 2-12
Circle Yukon River	-0.75 2-5	-0.76 1-22	-0.74 2-12
Crooked Creek Kuskokwim River	-0.84 11-26	-0.76 2-5	-0.80 11-26
Dawson Yukon River	-0.77 10-23	-0.67 1-22	-0.75 10-23
Eagle Yukon River	-0.77 10-23	-0.79 1-22	-0.76 1-29
Emmonak Yukon River	-0.76 2-5	-0.76 1-29	-0.71 4-16
Fort Yukon Yukon River	-0.72 10-23	-0.59 2-5	-0.72 10-23
Galena Yukon River	-0.79 11-19	-0.75 1-15	-0.80 4-16
Holy Cross Yukon River	-0.75 1-8	-0.77 1-8	-0.72 1-8
Hughes Koyukuk River	-0.81 1-1	-0.78 1-15	-0.78 4-2
Kaltag Yukon River	-0.84 12-3	-0.77 12-3	-0.86 1-15
Kobuk Kobuk River	-0.81 1-8	-0.62 4-16	-0.81 1-8
McGrath Kuskokwim River	-0.81 3-26	-0.81 2-5	-0.82 4-9
Mountain Village Yukon River	-0.72 1-29	-0.76 2-5	-0.69 2-19
Nenana Tanana River	-0.71 1-1	-0.73 2-5	-0.72 1-1
Nikolai Kuskokwim River	-0.75 2-12	-0.70 2-5	-0.74 1-15
Red Devil Kuskokwim River	-0.79 12-3	-0.80 2-5	-0.78 12-3
Ruby Yukon River	-0.83 4-9	-0.78 1-15	-0.86 4-16
Russian Mission Yukon River	-0.71 11-26	-0.72 12-10	-0.68 12-3
Tanana Yukon River	-0.76 1-22	-0.70 2-5	-0.77 11-26